Published in final edited form as:
Neuroimage. 2010 May 1; 50(4): 1456–1463. doi:10.1016/j.neuroimage.2010.01.053.

High-resolution fMRI mapping of ocular dominance layers in cat lateral geniculate nucleus

Nanyin Zhang[1,2], **Xiao-Hong Zhu**[1], **Yi Zhang**[1], **Jae-keun Park**[1,3], and **Wei Chen**[1,*]

[1] Center for Magnetic Resonance Research, Department of Radiology, University of Minnesota Medical School, Minneapolis, Minnesota

[2] Center for Comparative Neuroimaging, Department of Psychiatry, University of Massachusetts Medical School, Worcester, Massachusetts

[3] Department of Biomedical Engineering, Emory University, Atlanta Georgia

Abstract

In this work, we exploited the superior capability of high-resolution functional magnetic resonance imaging (fMRI) for functional mapping of ocular dominance layer (ODL) in the cat lateral geniculate nucleus (LGN). The stimulus-evoked neuronal activities in the LGN ODLs associated with contralateral- and ipsilateral-eye visual inputs were successfully differentiated and mapped using both blood-oxygenation-level dependent (BOLD)-weighted and cerebral blood volume (CBV)-weighted fMRI methods. The morphology of mapped LGN ODLs was in remarkable consistency with histology findings in terms of ODL shape, orientation, thickness and eye-dominance. Compared with the BOLD signal, the CBV signal provides higher reproducibility and better spatial resolvability for function mapping of LGN because of improved contrast-to-noise ratio and point-spread function. The capability of fMRI for non-invasively imaging the functional sub-units of ODL in a small LGN overcomes the limitation of conventional neural-recording approach, and it opens a new opportunity for studying the critical roles of LGN in brain function and dysfunction at the fine scale of ocular dominance layer.

Keywords

functional MRI (fMRI); lateral geniculate nucleus (LGN); ocular dominance layer (ODL); blood-oxygenation-level-dependent (BOLD); cerebral blood volume (CBV)

Introduction

The lateral geniculate nucleus (LGN) is an important thalamic structure with multiple ocular dominance layers in relaying visual information from the retina to primary visual cortex (V1). Neurons within each LGN ocular dominance layer (ODL) are exclusively monocular in receiving retinal inputs (Hubel and Wiesel, 1972). Morphologically, the LGN ODLs vary from specie to specie. The human and primate have six monocular ODLs with layers 2, 3 and 5

*Corresponding Author: Wei Chen, PhD, Center for Magnetic Resonance Research (CMRR), Departments of Radiology and Biomedical Engineering, University of Minnesota School of Medicine, 2021 6th Street S.E., Minneapolis, MN 55455, Phone: (612) 868-8303, Fax: (612) 626-2004, wei@cmrr.umn.edu.

driven by the ipsilateral eye and layers 1, 4 and 6 driven by the contralateral eye. The cat LGN, on the other hand, has three monocular ODLs with layers A and C_M driven by the contralateral eye and layer A1 driven by the ipsilateral eye (Payne et al., 2002; Sanderson, 1971).

Although the relay function was once regarded as the only function of the LGN, later studies have suggested that LGN plays crucial roles in processing of visual information, binocular rivalry, visual attention, perception and cognition. It is thus of interest to map the functional activity in LGN *in vivo*. Up to date, the prevalent practice for this task is using the neural-recording approach, which suffers from invasiveness and incapability to provide spatial information of large-scale neuronal activity covering the entire LGN body. Moreover, most neuroimaging modalities are incapable of mapping the LGN activity because of the lack of sufficient spatial and/or temporal resolution (e.g., positron emission tomography) or limited penetration of imaging signal (e.g., optical imaging) into the deep brain region where LGN locates. In contrast, functional magnetic resonance imaging (fMRI) based on blood-oxygenation-level-dependent (BOLD) (Bandettini et al., 1992; Blamire et al., 1992; Frahm et al., 1992; Kwong et al., 1992; Ogawa et al., 1992) has been successfully applied to map LGN activation and its retinotopic organization (Buchel et al., 1997; Chen et al., 1998b; Chen and Zhu, 2001; Chen et al., 1999; Grueschow et al., 2008; Kastner et al., 2004; Schneider et al., 2004). Moreover, the LGN activity was also mapped using the arterial spin labeling fMRI method in the human brain (Lu et al., 2008). However, mapping functional LGN activity at the more fundamental level of ocular dominance layer is challenging and has never been realized, due to the small ODL size and its deep brain location. This ability is extremely important in extending the LGN research with significantly more insights with respect to its function. This is because given the key role that LGN plays in the brain, the functional information from each ODL in LGN and other sub-cortical nuclei is crucial in understanding fundamental mechanisms of basic brain functions including general principles of cortico-thalamic circuitry and neural network, mechanism and architecture underlying the processing of complex visual input.

In the present study, we exploited the feasibility of functionally mapping the ODLs in the cat LGN. The LGN ODLs associated with contralateral- and ipsilateral-eye inputs were differentiated and mapped using the BOLD signal. Moreover, the BOLD-weighted ODL maps were compared to the ODL maps obtained using another fMRI approach based on the cerebral blood volume (CBV) measurement using the intravascular contrast agent of super-paramagnetic particles. Since the CBV signal has a better spatial resolution suitable for sub-millimeter fMRI mapping (Sheth et al., 2004; Zhao et al., 2006), the comparison result was used to examine the spatial specificity and spatial resolvability of BOLD-weighted fMRI LGN ODL maps. To examine the fMRI reliability, we also quantified the mapping reproducibility.

Materials and Methods

Animal Preparation

Eight cats (body weight: 1.5±0.3 kg) were used in this study. The animals were initially anesthetized with mixture of ketamine (15.0 mg/kg, i.v.) and xylazine (2.5 mg/kg). After oral intubation and mechanical ventilation (30–33 stokes/min), anesthesia was switched to 0.9–1.2% isoflurane in a N_2O/O_2 mixture of 70:30 volume ratio throughout the experiment. The pupils of the cat were dilated with drops of atropine sulfate solution. Contact lenses were emplaced to protect the corneas from drying. The animal was placed in a cradle and restrained in normal postural position. Head position of cat was fixed by a home-built head holder with mouth and ear bars to avoid head movement. Cat rectal temperature was monitored with a temperature sensor (PhysiTemp Instrument, Clifton, New Jersey) and maintained at 38.3±0.3 °C by using a heated circulating water blanket. The end-tidal CO_2 was monitored (Capnomac Ultima; Instrumentarium Corp. Finland) and maintained at normal conditions (between 3.8%

and 4.2%) by adjusting respiratory rate and tidal volume. The Institutional Animal Care and Use Committee of the University of Minnesota approved all animal surgical procedures and experimental protocol.

Experiment procedure and data acquisition

Visual stimulation (high-contrast flashing light generated by a pair of red LED goggles from Grass Instruments, Quincy, MA) was presented monocularly to either the left or right eye. Extra care was taken to ensure no light leakage across the eyes.

All the fMRI studies were performed on a 9.4 tesla (T) horizontal magnet (Magnex Scientific, UK) interfaced with a Varian INOVA console (Varian Inc., Palo Alto, CA). A half-volume radiofrequency (RF) coil based on the microstrip transmission line resonator coil design (Zhang et al., 2001; Zhang et al., 2005) was used to ensure adequate MRI detection sensitivity in the deep brain region where LGN is located. At first, multi-slice anatomical images were acquired using a conventional T_1-weighted TurboFLASH imaging method (Haase, 1990). To locate the image slice position optimal to mapping the LGN ODLs, a pilot fMRI run was conducted by acquiring multi-slice gradient-echo planar images (GE-PI) covering the LGN areas selected on the basis of the anatomic images. The parameters for the pilot fMRI run were: repetition time (TR) = 1000 ms; echo time (TE) = 14 ms; 5 adjacent axial slices without gaps; 1 mm slice thickness; field of view = 5cm×5 cm; 780μm×780μm in-plane spatial resolution. Single or multiple slices showing the strong LGN activation were selected for the subsequent ODL mapping experiments.

The LGN ODL mapping experiment was conducted using a block paradigm design. Each fMRI run was composed of two task blocks (15 image volumes per block) interleaved with three baseline blocks (15 image volumes per block). Within each task block, either the left eye or right eye of the cat was stimulated using the LED light flashing at 4 Hz. During the baseline block, the cat was in uniform darkness. The right-eye and left-eye stimulation tasks were arranged randomly across runs.

The BOLD-weighted fMRI data were obtained from all animals (n=8) using high-spatial-resolution GE-EPI images (coronal orientation) with the parameters: TR = 4000 ms; TE = 20 ms; field of view = 5cm×5cm; 390μm×390μm in-plane spatial resolution; 1 mm slice thickness; no gap between slices; and four segments for acquiring one GE-EPI slice.

In four of eight cats, which participated in non-survival studies (in compliance with the approved experimental protocol for the use of intravascular contrast agent), CBV-based fMRI data (n=4) were acquired after the BOLD-weighted fMRI measurements using the injection of the intravascular contrast agent of mono-crystalline iron oxide nanoparticle (MION). The same GE-EPI acquisition parameters were applied except that TE was minimized to 8 ms to suppress the BOLD contribution. MION injection was composed of a bolus (10 mg Fe/kg) followed by a constant-rate infusion (10 mg Fe/kg/hour) for compensating the MION dilution, thus, maintaining stable blood MION concentration and baseline CBV fMRI signal level for the period of imaging acquisition.

Twenty-four runs were separately acquired for obtaining BOLD- and CBV-weighted fMRI data from the same animal.

Data analysis

All the fMRI data analysis was performed using STIMULATE (Stimulate, Center for Magnetic Resonance Research, University of Minnesota) (Strupp, 1996) and Matlab (The Mathworks Inc., Natick, MA, USA). The fMRI time series were selectively averaged from multiple runs for each task. Based on the averaged time series of each task, an activation map was generated

using the time-shifted cross correlation (CC) method (Bandettini et al., 1993; Xiong et al., 1995). A boxcar function was chosen as the reference function and the threshold was set at CC coefficient > 0.3 (equivalent to $p < 0.01$). Potential large-vessel contamination was removed by excluding pixels containing low EPI signal intensity and large signal variation (Chen et al., 1998b; Chen and Zhu, 2001; Chen et al., 1999). The mmajor difference that this procedure causes is at the cortical surfaces where large vessels are located. For each activated pixel, the amplitude of the fMRI response was calculated as percentage change relative to the baseline signal.

The subtraction method, in which the BOLD activity in response to one-eye stimulation is subtracted from that to the fellow-eye stimulation, was applied to improve the spatial resolvability of fMRI. The same method was used in mapping ocular dominance column in human to correct for the bleeding signal induced by the intrinsic BOLD point spread function (Menon and Goodyear, 1999; Shmuel et al., 2007; van Gelderen et al., 2005). Specifically, at the corresponding activated pixel, the fMRI amplitude at the left-eye stimulation condition was subtracted from that at the right-eye stimulation condition. After subtraction, pixels with a positive value were designated as being located at right-eye ODLs while pixels with a negative value were designated as being located at left-eye ODLs for BOLD data. Conversely, pixels with a positive value were designated as being located at left-eye ODLs while pixels with a negative value were designated as being located at right-eye ODLs for CBV data owing to their opposite effects on the fMRI signal changes, i.e., resulting in an EPI signal reduction when CBV increases during brain activation.

The presented LGN ODL maps (except Figure 6 for comparing pixel-to-pixel reproducibility) were interpolated to an in-plane spatial resolution of $195 \times 195\ \mu m^2$.

Results

Functional Mapping of LGN ODLs

Figure 1 demonstrates typical functional maps of LGN ODLs based on BOLD-weighted fMRI data, in which green and red color indicates that the fMRI signal is dominantly activated by the right and left-eye stimulation, respectively. As shown in the maps, the LGN ODLs can be clearly observed and identified bilaterally in two hemispheres. Three major monocular ODLs in LGN (i.e., layers C_M, A1 and A in Figure 1) are reliably differentiated as delineated by the white profiles along the boundary of different colors (or different LGN ODLs). All three ODLs largely run horizontally. The tail of layer A extends more laterally compared to layers C_M and A1 and turns its orientation towards inferior at the lateral ends of layers A1 and C_M. As expected, the fMRI signal in layers C_M and A is activated by contralateral-eye stimulation while the fMRI signal in layer A1 is activated by ipsilateral-eye stimulation. All these morphologic elements determined by the mapped ODLs including layer shape, orientation and eye dominance are consistent with the literature based on the histological measurement (Lee et al., 1999;Sanderson, 1971). Figures 1A and 1B present the LGN ODL maps in two adjacent coronal image slices from the same cat based on BOLD-weighted fMRI data. All ODL structures can be readily separated in both image slices showing consistent eye dominance and similar ODL orientation between them. Meanwhile, a smooth change in shape for each corresponding ODL can be observed between these two adjacent fMRI slices, illustrating a continuous structural transformation of the LGN ODLs along the direction from anterior to superior side. This shape change in space is also consistent with the histological results (Sanderson, 1971).

Figure 2 compares the functional LGN ODL maps that were created using the BOLD- and CBV-weighted fMRI signals, respectively, acquired at the same image slice position. Both BOLD and CBV maps were capable of differentiating the LGN ODL structures. The position

of each corresponding LGN ODL is almost identical between the BOLD and CBV maps. The shape and orientation of each corresponding ODL are also similar. However, there is a systematic difference in thickness of the corresponding ODL between the BOLD and CBV fMRI maps. The thickness of layers A and C_M is wider in the BOLD map than that in the CBV map, whereas that of layer A1 is remarkably narrower in the BOLD map compared to the CBV map. This deviation results from the difference in the width of the intrinsic point spread function between the BOLD and CBV signals, which was investigated and is discussed in the next section.

Gradual shape transformation of each LGN ODL across the whole LGN body is illustrated in Figure 3, in which the LGN ODL maps from all cats, including both types of fMRI maps based on BOLD and CBV signals, are shown after co-registration of image slice positions. Although only a portion of LGN body was selected to map the ODL structures in each fMRI session, with a large enough inter-subject sample size, we were able to cover the entire LGN body across all fMRI sessions. For each image slice, its position relative to the most posterior end of the LGN body (indicated by the number on each map) was identified. This positioning procedure was accomplished by comparing and matching anatomical landmarks in the T_1-weighted anatomical image of this slice with those in a full set of three-dimensional (3D) high-resolution T_1-weighted anatomical images that covered the entire LGN body (see Supplemental Figure S1). According to this relative coordinate, we compared the LGN ODL map revealed by fMRI with the LGN ODL outlines (black color) drawn from a histological image at the corresponding image position (see Supplemental Figure S2, adapted from the reference of (Sanderson, 1971)) shown on the left side of each fMRI map in Figure 3. White profiles in each fMRI map are LGN body boundaries drawn from the corresponding anatomical image. Figure 3 shows that the LGN ODL shapes, the geometries and sizes of the entire LGN body as revealed by fMRI maps at given image slice positions are highly consistent with that manifested by histology and anatomic MRI, showing a gradual and continuous LGN shape transformation from the posterior to anterior LGN body. These results clearly demonstrate that the functional mapping of LGN ODL structure using fMRI is robust and reliable. Moreover, these results indicate that fMRI has the potential to functionally map the 3D LGN ODL structures covering the entire LGN body.

Distinct Characters between BOLD- and CBV-weighted fMRI Signals

Figure 4 plots the traces of BOLD and CBV signals along the brain regions marked by the white dash lines across the activated LGN body. The red traces plot the profiles of CBV (left panel, Figure 4A) and BOLD (right panel, Figure 4B) signals induced by the ipsilateral-eye stimulation showing substantial signal changes in the layer A1. The green traces plot the profiles of BOLD and CBV signals induced by the contralateral-eye stimulation showing substantial signal changes in the layers A and C_M. The LGN activation resulted in opposite signal changes: i.e., an increase in the BOLD signal and a decrease in the CBV signal due to distinct mechanisms underlying these two neuroimaging modalities. The blue traces are the profiles after subtracting the contralateral-eye activity from the ipsilateral-eye activity for the BOLD signal and vice versa for the CBV signal. The subtraction result was used to designate each activated pixel to the corresponding ODL. Clearly, the BOLD profiles from the contralateral-eye activity are considerably wider than the corresponding CBV profiles, suggesting that the amount of “bleeding” signals from the contralateral-eye activity trespassing into the territory of the ipsilateral-eye ODL (i.e., A1) is greater in BOLD data than in CBV data. Therefore, at territory boundaries of the ipsilateral-eye ODL, the summation of the bleeding BOLD signals from the two neighboring contralateral-eye ODL activity has a higher chance to dominate over the signal from the ipsilateral-eye ODL activity. As a result, BOLD maps tend to underestimate the thickness of the ipsilateral ODL (inside) and overestimate that of the contralateral ODL (outside) compared to CBV maps.

The distinct bleeding effect can also be observed from the BOLD and CBV signals inside the one-eye dominant ODL activated by the fellow-eye stimulation. Figure 5 clearly shows a substantial bleeding BOLD signal detected in the left-eye dominant ODL during the right-eye stimulation. Similarly, in the right-eye dominant ODLs, there is also considerable bleeding BOLD signal during left-eye stimulation. This bleeding effect, in contrast, is not evident in the CBV time courses. These results confirm that the intrinsic point spread function of the BOLD signal is significantly wider than that of the CBV signal. Nevertheless, the BOLD signal is still able to differentiate the ODL structures of the LGN using high-resolution fMRI with the subtraction method.

Quantitative Evaluation of Reproducibility of LGN ODL Maps

Figure 6 examines the reproducibility of both BOLD-weighted and CBV-weighted LGN ODL maps (all maps in Figure 6 are shown in the original fMRI spatial resolution without interpolation). Both types of fMRI data acquired in the same session (Figure 6A) were randomly split into two halves (Figure 6B and Figure 6C). LGN ODL maps created by the first and second halves of BOLD data are largely reproducible. In comparison, the corresponding CBV-based LGN ODL maps are more similar to each other indicating that the CBV signal has a higher reproducibility rate in mapping the LGN ODL structure. Quantitatively, the reproducibility rate in designating all activated pixels to either contralateral-eye or ipsilateral-eye ODLs for the BOLD signal was 0.76 when averaged from all cats ($p < 0.001$, paired t-test against 0.5) and that for CBV data is 0.84 ($p < 0.001$, paired t-test against 0.5). These results suggest that the LGN ODL maps based on BOLD and CBV fMRI signals are statistically reproducible and reliable.

Figure 7 plots the amplitude difference of fMRI signals acquired between the right-eye and left-eye stimulation conditions of the corresponding pixels in the subtraction maps created from the first and second halves of data. The left panels are plots from one representative cat and the right panels are plots from all cats. The upper panels are plots for the BOLD data and the lower panels are the plots for the CBV data. All plots show significant correlation of amplitude differences between the two halves of data. These results, together with significant reproducibility rates between the fMRI maps independently created from two halves of data, unequivocally indicate again that the LGN ODL maps created by BOLD and CBV data are reproducible. Since the BOLD signal in the “bleeding” zone was decoupled with the CBV signal, the comparison between the BOLD and CBV correlation within the activated LGN was not pursued.

Discussion

It has been found that the LGN plays essential roles in processing of visual information, binocular rivalry, visual attention, perception and cognition, which is much beyond the relay function. O’Connor et al found that directed attention to a spatial location modulated neuronal activity in LGN in several ways: it enhanced neural responses to attended stimuli, attenuated responses to ignored stimuli, and increased baseline activity in the absence of visual stimulation (O’Connor et al., 2002). This finding is consistent with another study showing attention effects on the human magno- and parvo-cellular LGN pathways (Schneider and Kastner, 2009).

Haynes et al, together with other groups, reported that neuronal activities in LGN strongly correlated with the subjects’ percept during the period of binocular rivalry and was sensitive to the visual stimulation contrast (Grueschow et al., 2008; Haynes et al., 2005; Wunderlich et al., 2005), suggesting that LGN is actively involved in visual perception and rivalry. Moreover, it has been shown that the response mode of LGN can switch between ‘tonic’ and ‘burst’ modes: when geniculate cells are in the tonic mode, LGN faithfully transmits the visual information from the retina to the visual cortex; whereas when geniculate cells are in the burst mode, the

transmission of visual information is not as effective (Sherman, 2001; Sherman and Guillery, 1996, 2002). This finding suggests that LGN may serve as a gatekeeper in control of selective transmission of visual information. This type of control is tightly linked to visual awareness and attention (McAlonan et al., 2008; Sherman and Guillery, 1996). Also LGN is considerably activated during visual imaginary in the human in the absence of external visual input (Chen et al., 1998a), indicating that the function of LGN might be extraordinarily influential in high-level cognitive function. Taken together, all these studies manifest that the function of LGN goes far beyond simply relaying visual information and is the key to visual functions at all levels.

In the present work, we demonstrate the superior capability of high-resolution fMRI for non-invasively mapping the LGN ODL structures at high field (9.4T). The LGN ODLs associated with contralateral- and ipsilateral-eye inputs have been successfully differentiated using both BOLD- and CBV-weighted fMRI signals. The morphology of mapped LGN ODLs is in consistency with histological data in terms of ODL shape, orientation and eye-dominance. Compared to the maps created by the BOLD signal, the CBV-weighted fMRI offers better mapping reproducibility which is evident with higher reproducibility rate of activated pixels and higher correlation coefficient of subtracted signal amplitudes between two halves of data acquired in the same session, and better spatial resolvability due to a narrower intrinsic CBV point spread function. This is in accordance with the notion that CBV-weighted fMRI signal measured by MION contrast agent has a better contrast to noise ratio (CNR) compared to the BOLD-weighted fMRI signal (Zhao et al., 2006). We estimated the CNR in our experiment. After MION injection, image signal intensity at the LGN region drops to 67% of the pre-injection level. However, the activation-induced signal change is larger by a factor of 2.2 for the CBV signal (acquired after MION injection) compared with the BOLD signal (acquired before MION injection). As a result, the CNR of the CBV-weighted signal is approximately 48% higher than that of the BOLD signal. This result agrees with the literature report of approximately 1.5 times (or 50%) higher parenchymal sensitivity of CBV-weighted fMRI than that of BOLD-weighted fMRI (Zhao et al., 2006).

In addition to higher sensitivity in mapping the LGN ODL structures, the CBV signal also offers a better spatial resolvability. This is because activation-related CBV signal change is mainly attributed to parenchyma, not microvasculature (Zhao et al., 2005). Therefore, the CBV change accompanied with local neuronal activity should reflect the activity of microvasculature (Kuschinsky, 1996). As a result, the point spread function of the CBV signal should be similar to that of perfusion and substantially narrower than that of the gradient-echo BOLD signal, which is contributed by vessels from all sizes. It has to be noted that since in a compact brain tissue structure such as the sub-cortical LGN, it does not have the stereotypical vascular structure characteristic of the surface cortex. As a result, the difference in the point spread function between the BOLD and CBV signals observed in the present study most likely result from the vessels of intermediate sizes (Turner, 2002); thus, it is expected to be relatively small compared to the cortical regions (Zhao et al., 2005). This notion is consistent with our observation showing the feasibility of both BOLD and CBV fMRI approaches for mapping the LGN ODLs based on the subtraction method.

It has been reported from a morphological study that the ipsilateral-eye LGN ODLs take approximately 28% of the whole LGN volume in the cat (Lee et al., 1999). This volume fraction was also measured in the present fMRI study by calculating the ratio of the number of the activated pixels designated to ipsilateral-eye LGN ODLs divided by that of all activated LGN pixels. We found that for the functional LGN ODL maps based on the CBV-weighted signal, this ratio was 26.3%, which is in excellent consistency with the literature report. In contrast, for the LGN ODL maps based on the BOLD-weighted signal, this ratio was significantly lowered to 16.2% ($p < 0.05$, paired t-test). This discrepancy is in line with the aforementioned

notion that the LGN ODL maps based on BOLD signal tends to underestimate the thickness and volume of ipsilateral-eye ODL (A1) while overestimate those of contralateral-eye ODLs (C_M and A), as a wider point spread function of the BOLD signal induces more severe bleeding signal in the ipsilateral-eye ODLs from the neighboring contralateral-eye ODLs. This mismatch in ODL size owing to the intrinsic point spread function of the hemodynamic response is negligible in CBV maps as revealed by Figure 5.

The ability of obtaining functional ODL activity in LGN makes it possible to map the visual neural network at a more fundamental level. It has been well demonstrated that functional activity of the columnar structure in the visual cortex can be mapped using fMRI (Cheng et al., 2001; Menon and Goodyear, 1999; Yacoub et al., 2007). The anatomic and functional connections between the ocular dominant layers in LGN and the corresponding ocular dominance columns in V1 constitute a fundamental neural network of the visual system and should be tightly linked to numerous visual functions. Simultaneously mapping functional activities in the LGN ODL structure and ocular dominance columnar structure in the visual cortex should provide new insights regarding visual information processing along the cortico-thalamic network under specific stimulation condition.

In summary, we have demonstrated the high-resolution fMRI maps of ocular dominance layer structures in the cat LGN with superior quality. This capability overcomes a number of limitations faced by the conventional neural-recording technique and other neuroimaging methods; and it will pave the fMRI research for understanding the central roles of LGN on various brain functions. Finally, the same fMRI approaches should be suitable for functional mapping of sub-units down to the laminar level in other sub-cortical nuclei.

Supplementary Material

Refer to Web version on PubMed Central for supplementary material.

Acknowledgments

We thank Dr. Kamil Ugurbil for support and Dr. Xiaoliang Zhang for his help in RF coil design and construction. This work was supported in part by NIH grants of NS041262, EB000329, EB000513, NS057560, P41 RR08079 and P30NS057091; and the Keck Foundation.

References

Bandettini PA, Jesmanowicz A, Wong EC, Hyde JS. Processing strategies for time-course data sets in functional MRI of the human brain. Magn Reson Med 1993;30:161–173. [PubMed: 8366797]

Bandettini PA, Wong EC, Hinks RS, Tikofsky RS, Hyde JS. Time course EPI of human brain function during task activation. Magn Reson Med 1992;25:390–397. [PubMed: 1614324]

Blamire AM, Ogawa S, Ugurbil K, Rothman D, McCarthy G, Ellermann JM, Hyder F, Rattner Z, Shulman RG. Dynamic mapping of the human visual cortex by high-speed magnetic resonance imaging. Proc Natl Acad Sci USA 1992;89:11069–11073. [PubMed: 1438317]

Buchel C, Turner R, Friston K. Lateral geniculate activations can be detected using intersubject averaging and fMRI. Magn Reson Med 1997;38:691–694. [PubMed: 9358440]

Chen W, Kato T, Zhu XH, Ogawa S, Tank DW, Ugurbil K. Human primary visual cortex and lateral geniculate nucleus activation during visual imagery. Neuroreport 1998a;9:3669–3674. [PubMed: 9858377]

Chen W, Kato T, Zhu XH, Strupp J, Ogawa S, Ugurbil K. Mapping of lateral geniculate nucleus activation during visual stimulation in human brain using fMRI. Magn Reson Med 1998b;39:89–96. [PubMed: 9438442]

Chen W, Zhu XH. Correlation of activation sizes between lateral geniculate nucleus and primary visual cortex in humans. Magn Reson Med 2001;45:202–205. [PubMed: 11180426]

Chen W, Zhu XH, Thulborn KR, Ugurbil K. Retinotopic mapping of lateral geniculate nucleus in humans using functional magnetic resonance imaging. Proc Natl Acad Sci U S A 1999;96:2430–2434. [PubMed: 10051659]

Cheng K, Waggoner RA, Tanaka K. Human ocular dominance columns as revealed by high-field functional magnetic resonance imaging. Neuron 2001;32:359–374. [PubMed: 11684004]

Frahm J, Bruhn H, Merboldt KD, Hanicke W. Dynamic MR imaging of human brain oxygenation during rest and photic stimulation. J Magn Reson Imag 1992;2:501–505.

Grueschow M, Rieger J, Stadler J, Tempelmann C, Heinze HJ, Speck O, Haynes JD. Topography of responses to colour and luminance in human subcortical visual pathways as revealed by high-resolution fMRI at 7T. Journal of Vision 2008;8:959.

Haase A. Snapshot FLASH MRI. Applications to T_1, T_2, and chemical-shift imaging. Magn Reson Med 1990;13:77–89. [PubMed: 2319937]

Haynes JD, Deichmann R, Rees G. Eye-specific effects of binocular rivalry in the human lateral geniculate nucleus. Nature 2005;438:496–499. [PubMed: 16244649]

Hubel DH, Wiesel TN. Laminar and columnar distribution of geniculo-cortical fibers in the macaque monkey. J Comp Neurol 1972;146:421–450. [PubMed: 4117368]

Kastner S, O'Connor DH, Fukui MM, Fehd HM, Herwig U, Pinsk MA. Functional imaging of the human lateral geniculate nucleus and pulvinar. J Neurophysiol 2004;91:438–448. [PubMed: 13679404]

Kuschinsky, W. Regulation of cerebral blood flow: an overview. Johns Libbey & Company Ltd; London: 1996.

Kwong KK, Belliveau JW, Chesler DA, Goldberg IE, Weisskoff RM, Poncelet BP, Kennedy DN, Hoppel BE, Cohen MS, Turner R, Cheng HM, Brady TJ, Rosen BR. Dynamic magnetic resonance imaging of human brain activity during primary sensory stimulation. Proc Natl Acad Sci USA 1992;89:5675–5679. [PubMed: 1608978]

Lee I, Kim J, Lee C. Anatomical characteristics and three-dimensional model of the dog dorsal lateral geniculate body. Anat Rec 1999;256:29–39. [PubMed: 10456983]

Lu K, Perthen JE, Duncan RO, Zangwill LM, Liu TT. Noninvasive measurement of the cerebral blood flow response in human lateral geniculate nucleus with arterial spin labeling fMRI. Hum Brain Mapp 2008;29:1207–1214. [PubMed: 17712783]

McAlonan K, Cavanaugh J, Wurtz RH. Guarding the gateway to cortex with attention in visual thalamus. Nature 2008;456:391–394. [PubMed: 18849967]

Menon RS, Goodyear BG. Submillimeter functional localization in human striate cortex using BOLD contrast at 4 Tesla: implications for the vascular point-spread function. Magn Reson Med 1999;41:230–235. [PubMed: 10080267]

O'Connor DH, Fukui MM, Pinsk MA, Kastner S. Attention modulates responses in the human lateral geniculate nucleus. Nat Neurosci 2002;5:1203–1209. [PubMed: 12379861]

Ogawa S, Tank DW, Menon R, Ellermann JM, Kim SG, Merkle H, Ugurbil K. Intrinsic signal changes accompanying sensory stimulation: functional brain mapping with magnetic resonance imaging. Proc Natl Acad Sci USA 1992;89:5951–5955. [PubMed: 1631079]

Payne, B.; Sande, MA.; Gilbert, DN.; Moellering, RC.; Peters, A. The Cat Primary Visual Cortex. Academic Press; San Diego: 2002.

Sanderson KJ. The projection of the visual field to the lateral geniculate and medial interlaminar nuclei in the cat. J Comp Neurol 1971;143:101–108. [PubMed: 5097579]

Schneider KA, Kastner S. Effects of sustained spatial attention in the human lateral geniculate nucleus and superior colliculus. J Neurosci 2009;29:1784–1795. [PubMed: 19211885]

Schneider KA, Richter MC, Kastner S. Retinotopic organization and functional subdivisions of the human lateral geniculate nucleus: a high-resolution functional magnetic resonance imaging study. J Neurosci 2004;24:8975–8985. [PubMed: 15483116]

Sherman SM. Tonic and burst firing: dual modes of thalamocortical relay. Trends Neurosci 2001;24:122–126. [PubMed: 11164943]

Sherman SM, Guillery RW. Functional organization of thalamocortical relays. J Neurophysiol 1996;76:1367–1395. [PubMed: 8890259]

Sherman SM, Guillery RW. The role of the thalamus in the flow of information to the cortex. Philos Trans R Soc Lond B Biol Sci 2002;357:1695–1708. [PubMed: 12626004]

Sheth SA, Nemoto M, Guiou M, Walker M, Pouratian N, Hageman N, Toga AW. Columnar specificity of microvascular oxygenation and volume responses: implications for functional brain mapping. J Neurosci 2004;24:634–641. [PubMed: 14736849]

Shmuel A, Yacoub E, Chaimow D, Logothetis NK, Ugurbil K. Spatio-temporal point-spread function of fMRI signal in human gray matter at 7 Tesla. Neuroimage 2007;35:539–552. [PubMed: 17306989]

Strupp JP. Stimulate: A GUI based fMRI analysis software package. Neuroimage 1996;3:S607.

Turner R. How much cortex can a vein drain? Downstream dilution of activation-related cerebral blood oxygenation changes. Neuroimage 2002;16:1062–1067. [PubMed: 12202093]

van Gelderen P, CWHW, de Zwart JA, Cohen L, Hallett M, Duyn JH. Resolution and reproducibility of BOLD and perfusion functional MRI at 3.0 Tesla. Magn Reson Med 2005;54:569–576. [PubMed: 16086372]

Wunderlich K, Schneider KA, Kastner S. Neural correlates of binocular rivalry in the human lateral geniculate nucleus. Nat Neurosci 2005;8:1595–1602. [PubMed: 16234812]

Xiong J, Gao JH, Lancaster JL, Fox PH. Clustered pixels analysis for functional MRI activation studies of the human brain. Hum Brain Mapping 1995;3:287–301.

Yacoub E, Shmuel A, Logothetis N, Ugurbil K. Robust detection of ocular dominance columns in humans using Hahn Spin Echo BOLD functional MRI at 7 Tesla. Neuroimage 2007;37:1161–1177. [PubMed: 17702606]

Zhang X, Ugurbil K, Chen W. Microstrip RF surface coil design for extremely high-field MRI and spectroscopy. Magn Reson Med 2001;46:443–450. [PubMed: 11550234]

Zhang XL, Ugurbil K, Sainati R, Chen W. An inverted-microstrip resonator for human head proton MR imaging at 7 tesla. IEEE Biomed Engineering 2005;52:495–504.

Zhao F, Wang P, Hendrich K, Kim SG. Spatial specificity of cerebral blood volume-weighted fMRI responses at columnar resolution. Neuroimage 2005;27:416–424. [PubMed: 15923128]

Zhao F, Wang P, Hendrich K, Ugurbil K, Kim SG. Cortical layer-dependent BOLD and CBV responses measured by spin-echo and gradient-echo fMRI: insights into hemodynamic regulation. Neuroimage 2006;30:1149–1160. [PubMed: 16414284]

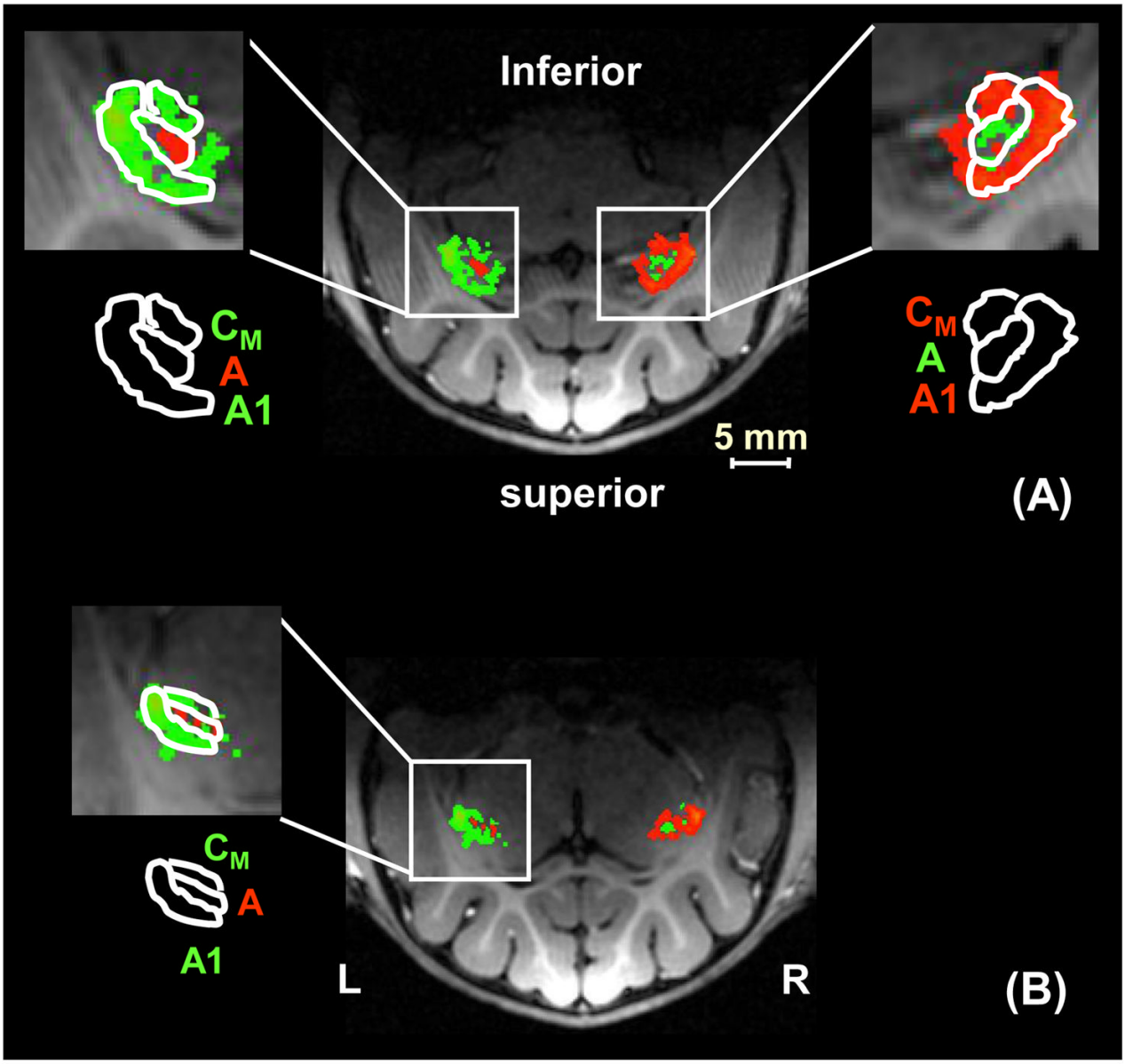

Figure 1.
Typical functional maps of LGN ODLs based on the BOLD-weighted fMRI measurement from two adjacent image slices shown in (A) and (B). Green color indicates that the fMRI signal is dominated by the right-eye stimulation; red color indicates that the fMRI signal is dominated by the left-eye stimulation. Three major monocular ocular dominance layers in LGN (i.e., layers C_M, A1 and A) can be reliably differentiated and identified, as depicted by white solid lines delineating the territory boundaries among the ODLs. The corresponding LGN ODLs in the two slices show consistent eye dominance, similar ODL orientation, and a smooth transformation in the LGN shape. The fMRI map in (B) is more anterior compared to the map in (A).

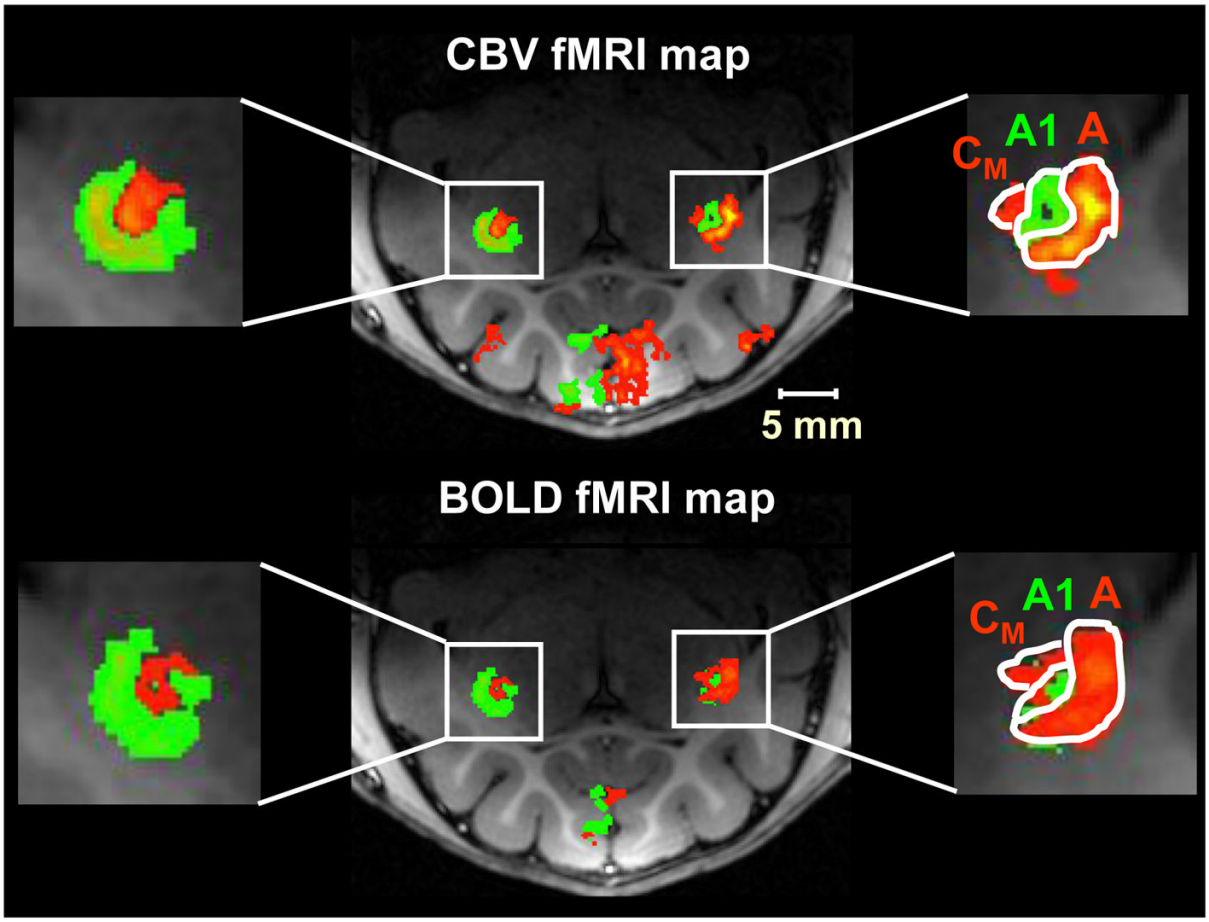

Figure 2.
Comparison of functional LGN ODL maps created from the BOLD and CBV signals. Both BOLD- and CBV-weighted fMRI maps are capable of differentiating the ODL structures in the LGN. The position of each corresponding ODL is almost identical between the BOLD and CBV maps. The shape and orientation of each corresponding ODL are also similar. However, the thickness of layers A and C_M is systematically wider in the BOLD map than that in the CBV map, while that of layer A1 is remarkably narrower.

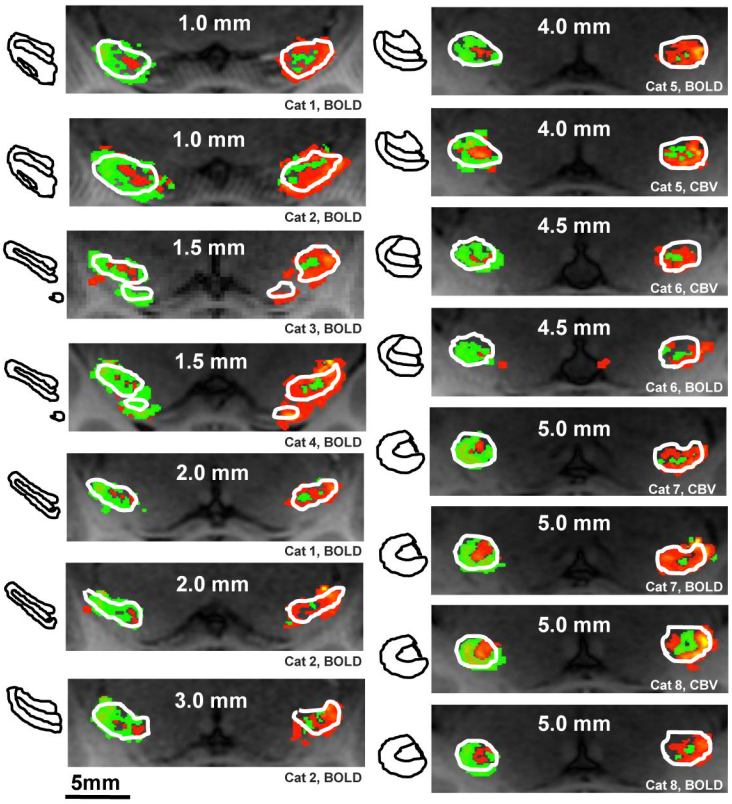

Figure 3.

Functional LGN ODL maps including both BOLD- and CBV-weighted fMRI maps from all cats. White profiles in each fMRI map are the LGN body boundaries drawn based on the corresponding anatomical image. For each image slice, its position relative to the most posterior end of LGN body (indicated by the number on each map) was identified by comparing anatomical landmarks in the anatomical image of the selected slice with those in a set of 3D high-resolution T_1-weighted anatomical images that covered the entire LGN body (Supplemental Figure S1). On the left of each fMRI map, the outlines (black color) of each LGN ODL at the corresponding image position were drawn based on histological images for comparison (Supplemental Figure S2, adapted from the reference of (Sanderson, 1971)). It is evident that the mapped LGN ODLs and whole LGN body by fMRI are in excellent agreement with the anatomic LGN architectures.

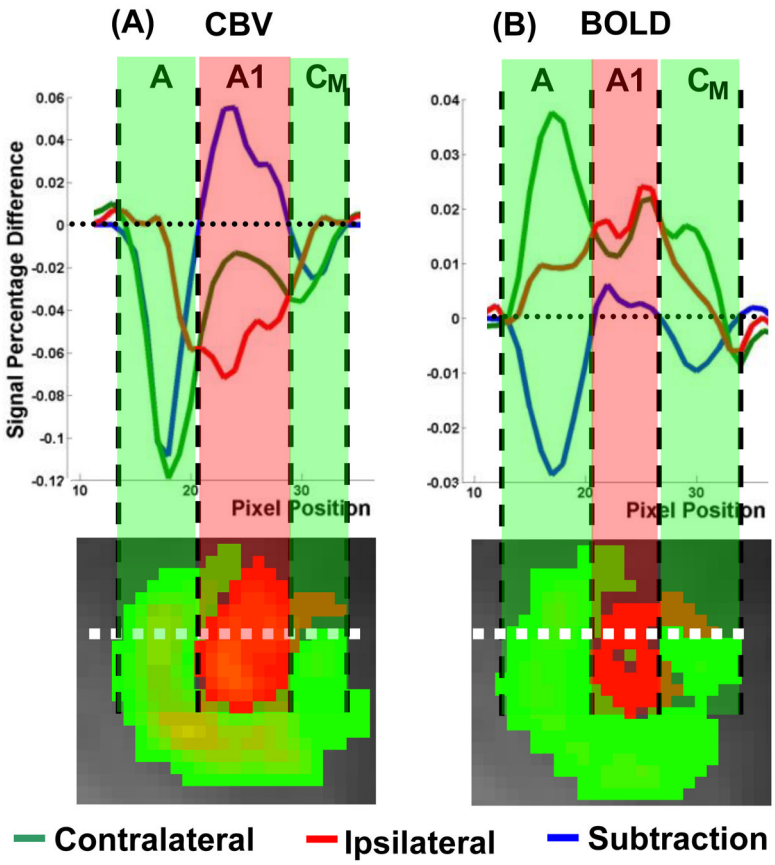

Figure 4.

Illustration of the effect of the point spread function in BOLD- and CBV-weighted fMRI signals on mapping the LGN ODL structures. The traces of BOLD and CBV signal are along the brain region marked by the white dash lines in the fMRI maps. The red traces indicate profiles of CBV (left panel, Figure 4A) and BOLD (right panel, Figure 4B) signals induced by ipsilateral-eye stimulation. The green traces are profiles of the BOLD and CBV signals induced by contralateral-eye stimulation. The blue traces are the profiles after subtracting the contralateral-eye activity from the ipsilateral-eye activity for the BOLD signal and vice versa for the CBV signal. These traces reveal well-defined CBV signal profiles across the adjacent LGN ODLs compared to BOLD signal profiles.

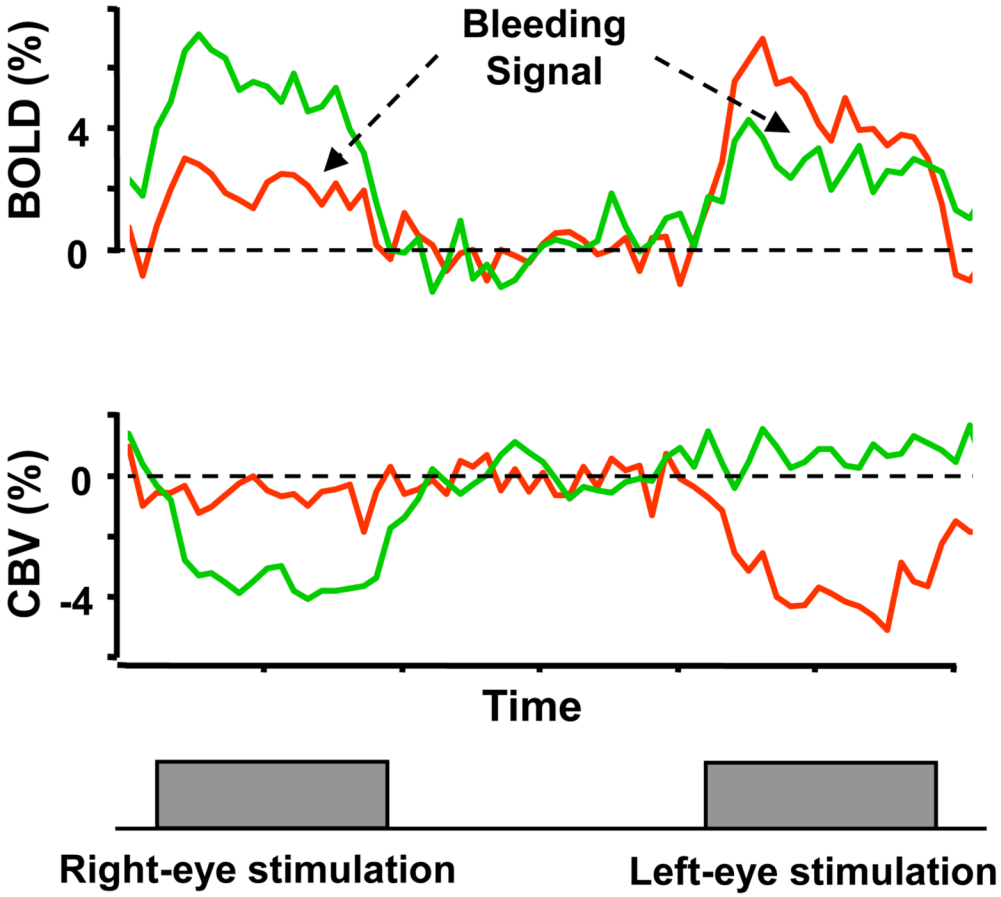

Figure 5.

Distinctive effect of the bleeding signals in BOLD (top panel) and CBV (bottom panel) time courses. The red traces indicate the BOLD or CBV signal profiles measured from the left-eye LGN ODLs; and the green traces indicate the BOLD or CBV signal profiles measured from the right-eye LGN ODLs during left- or right-eye stimulation. Bleeding signal in the BOLD time courses is substantial, yet it is negligible in the CBV time courses due to a better CBV spread point function.

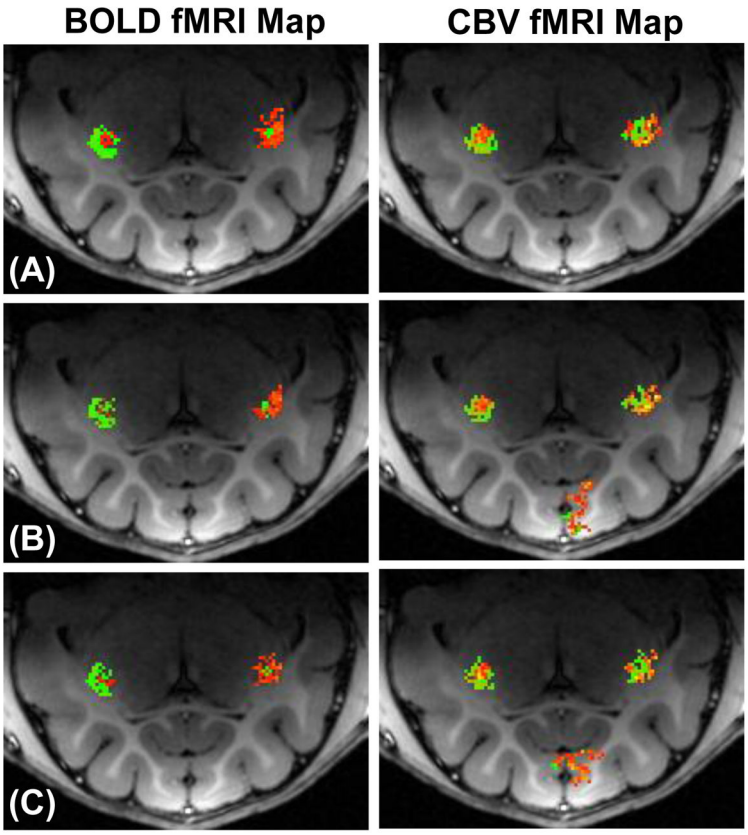

Figure 6.

Examining the reproducibility of LGN ODL mapping. Data are presented in the original imaging spatial resolution (390×390 μm^2). The BOLD (left panel) and CBV (right panel) data acquired within the same fMRI session were split into two halves, respectively. (A) The LGN ODL maps created from all the BOLD or CBV datasets. (B) The LGN ODL maps created from the first halves of fMRI datasets. (C) The LGN ODL maps created from the second halves of fMRI datasets. There are consistencies among the split fMRI maps.

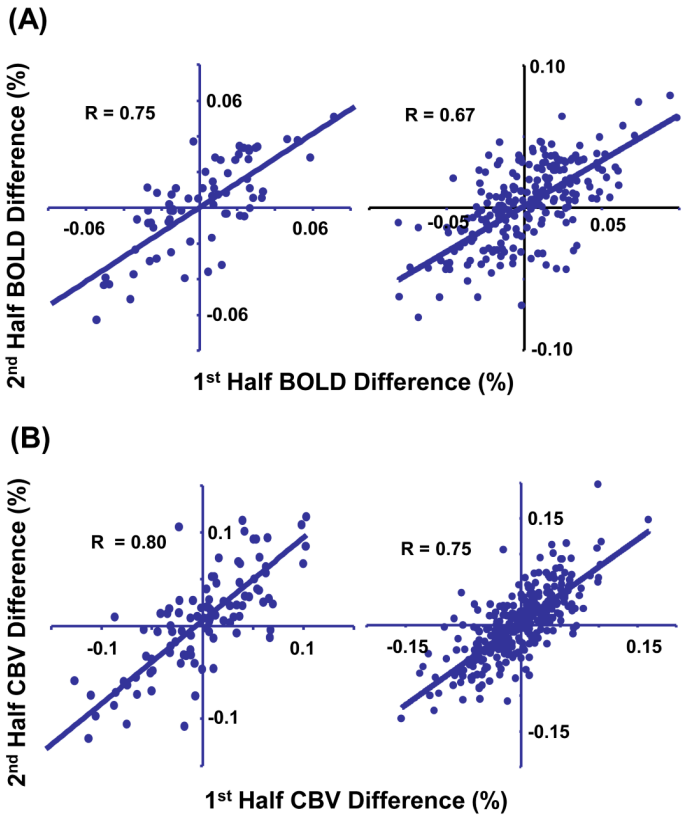

Figure 7.

Correlation of the first and second halves of fMRI data in the signal amplitude differences between the left- and right-eye stimulated LGN ODL activities. The sign of the amplitude differences can be positive or negative, and it depends on which eye being stimulated as demonstrated in Figure 5. The left panels are plots from one cat and the right panels are plots from all cats. The upper panels are plots for the BOLD data and the lower panels are plots for the CBV data.